Available online at www.sciencedirect.com
ScienceDirect
Remote Sensing of Environment 109 (2007) 285–294
Remote Sensing of Environment
www.elsevier.com/locate/rse

Dual-frequency altimeter signal from Envisat on the Amery ice-shelf

Pascal Lacroix [a,*], Benoit Legrésy [a], Richard Coleman [b], Monique Dechambre [c], Frédérique Rémy [a]

[a] CNRS-CNES-UPS-IRD, LEGOS, 14 av. Edouard Belin 31400 Toulouse, France
[b] University of Tasmania, Private Bag 78, TAS 7001 Hobart, Australia
[c] CETP, 10-12 av. de l'Europe, 78140 Velizy, France

Received 4 July 2006; received in revised form 27 November 2006; accepted 13 January 2007

Abstract

In Antarctica, radar altimeter measurements are sensitive to dielectric and penetration properties of the sensed medium (snow) such that the spacecraft's altitude can be biased. Since 2002, relatively low frequency radar measurements over the Amery Ice Shelf, east Antarctica, have been acquired using the Envisat dual frequency altimeter at S (3.2 GHz) and Ku (13.6 GHz) bands, which penetrate a few meters into the firn.

The altimeter signal is however modified in summer by the presence of snowfilled crevasses. Indeed, the specularity of the snow surfaces in summer makes the altimetric signal sensitive mostly to nadir echoes, that increases the ratio between the crevasse signal and the surrounding ice-shelf signal at nadir. Crevasses are distinguished by differences in backscattering behavior compared with the surrounding ice-shelf signal. Crevasses are characterized by a strong backscatter coefficient at Ku band and anomalies in the S band altitude estimation. These two characteristics make snowfilled crevasses detectable by the dual frequency altimeter of Envisat.

We first retrieve the geometric properties of the crevasses using a hyperbolic shape function, created by strong crevasse backscatter in the Ku waveform measurements. From this retrieved crevasse signal and further waveform analysis, we assess the properties of the snow surface and its sub-surface. The crevasse, due to its small size compared to the altimeter footprint, is found to be an excellent target to study snow properties of the ice-shelf.

The anomalies in the S band altitude measurements over crevasses can then be explained by the presence of a double echo in the S band waveforms. This echo is attributed to a reflection at the base of the snowbridge, where we see evidence of sub-surface echos in the individual altimeter waveforms. Based on this observation, a methodology is developed to estimate the thickness of the snowbridge. We calculate the penetration depths in the summer snow surface of the Amery at Ku band, that is found to be around 6 m.

Keywords: Radar altimetry; Antartica; Ice-shelf; Snow properties; Crevasses; Radar waves penetration

1. Introduction

The transmitted wave from radar altimeters penetrates several meters into the snow of Antarctica (Legrésy & Rémy, 1998), biasing the altimetric measurements. This penetration is primarily a function of the geophysical properties of the snow medium, and consequently the altimetric signal can be a rich source of information on properties of the Antarctic snow. The altimeter signal is influenced by snow surface properties: surface roughness at different spatial scales (Legrésy & Rémy, 1997; Legrésy et al., 1999; Ridley & Partington, 1988), or variation in snow surface density (Jun & Zwally, 2002), as well as sub-surface properties: snow grain scattering, or layers of high density contrast. Evidence of a sub-surface signal in the averaged altimetric waveform over the cold Antarctic plateau region has been pointed out by several studies (Arthern et al., 2001; Legrésy & Rémy, 1998). The higher spatial resolution ASIRAS data has proven the existence of sub-surface echoes in the individual waveforms over Greenland (Hawley et al., 2006). The altimetric data over ice sheets must be looked into detail to both correct for the altitude bias induced by the sub-surface signal, and study properties of the shallow snowpack. In this study we concentrate on snow properties and extract for the first time new information using dual frequency altimeters.

The ENVISAT altimeter, launched in 2002, operates at two frequencies (Ku band 13.6 GHz, and S band 3.2 GHz). A comparison between the two bands has already shown interesting

* Corresponding author. Tel.: +33 5 61 33 30 44; fax: +33 5 61 25 32 05.
E-mail address: lacroix@notos.cst.cnes.fr (P. Lacroix).

0034-4257/$ - see front matter © 2007 Elsevier Inc. All rights reserved.
doi:10.1016/j.rse.2007.01.007

sub-surface features (Legrésy et al., 2005). The two bands have very different interactions with the firn as their frequencies have different sensitivity to snow grain scattering, surface roughness, and varying penetration depth. The difference in their snow penetration properties can help us to investigate properties of the Antarctic snow, and to retrieve information about the firn.

In regions of Antarctica where melting occurs, the snow properties vary considerably, both spatially and temporally (especially seasonally). Over ice-shelves, surface melting (Fahnestock et al., 2002; Phillips, 1998) and warmer ocean temperatures (Scambos et al., 2000; Shepherd et al., 2003) both occur during summer. Snow on the ice-shelves is fully modified by summer melting, with melt ponds and melt streams developing at its surface (Phillips, 1998). The streams are drained and percolate into the snow to form icy layers and ice lenses. The high temperatures favor the formation of coarse snow grains. These summer conditions lead to a high temporal variability of the altimetric signal between summer and winter.

Our study focus here on the Amery Ice Shelf (AIS) (Fig. 1), where there has been a long history of field campaigns, and hence a large collection of in-situ data. On the AIS, the glacier flow is perturbated by the presence of a land area (Gillock Island) situated more than 100 km south of the ice-front, and

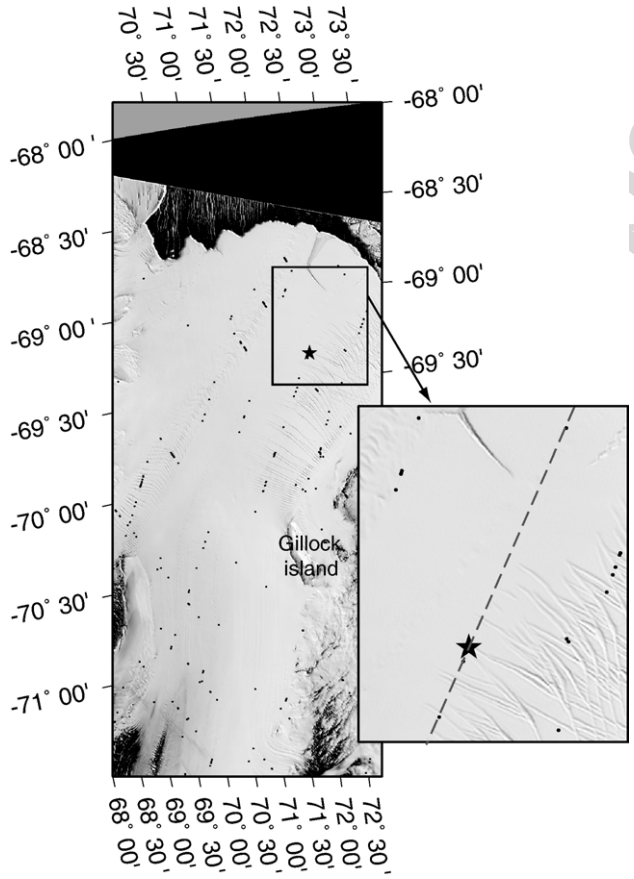

Fig. 1. MODIS image of the Amery ice-shelf, with a zoom on the northern part of the shelf. The marks show locations where the altitude difference measured between Ku and S bands is greater than 3σ. The dashed line corresponds to the satellite track exhibiting the hyperbola processed (its location is marked with a star shape).

Table 1
Envisat RA-2 altimeter signal characteristics

Parameter	Ku band	S band
Center frequency (GHz)	13.6	3.2
Antenna aperture at 3 dB	1.35°	5.5°
Bandwidth (MHz)	320	160
Time sampling (ns)	3.125	6.25
Vertical resolution in air (cm)	47	94

hence subject to a large divergence in the ice-shelf flow direction as it bends around the topographic obstacle. This divergence and the flow perturbation lead to the formation of large crevasses approximately at 90° to the flow direction. In many parts of the ice-shelf, precipitation is important, filling the crevasses with snow. When covered by a snowbridge, crevasses are not easily detectable and thus a significant hazard to ground surveys.

We will show here that the dual-frequency altimetric signal is modified by the presence of these large crevasses. Firstly, we focus on the altitude records and waveform analysis to show how the altimeter is sensitive to crevasse features. Next, we propose physical explanations to this phenomenon and use these signals to derive properties of the crevassing and the snow on the ice-shelf.

2. Observations

2.1. Background altimetry

Altimetry is particularly well designed for ice-shelf studies because of their flat aspect ratio (Rémy et al., 1989). The mean surface slope over the Amery Ice Shelf is between 0 and 1 m km^{-1}, hence the slope error is weak and can be neglected. The two datasets provided by the dual frequency altimeter of Envisat (Table 1) are fully comparable, once corrected for antenna gain. The acquisition time of the two altimeter frequencies is the same, and they are thus looking at exactly the same targets. The power return versus time t_e is called the altimetric waveform. The shape of this return signal is described by 4 main parameters: the height, the backscatter coefficient, the leading edge width and the trailing edge slope (see Legrésy et al., 2005). This waveform is digitized in several radar bins corresponding to a time sampling rate. The antenna footprint for one radar bin is a disk at the nadir of the satellite, and then becomes a ring of constant surface area S away from it. In the following, all the waveforms are corrected for the gain, so the S and Ku signals are fully comparable.

2.2. Height measurement analysis

We look at an altitude record over a crevassed zone of the ice-shelf (Fig. 2). The waveforms have been retracked to provide the altitude using the Ice2 algorithm (Legrésy et al., 2005), with the altimetric corrections applied to the two bands being equivalent except for the ionospheric correction. The ionospheric corrections have horizontal length scales of order

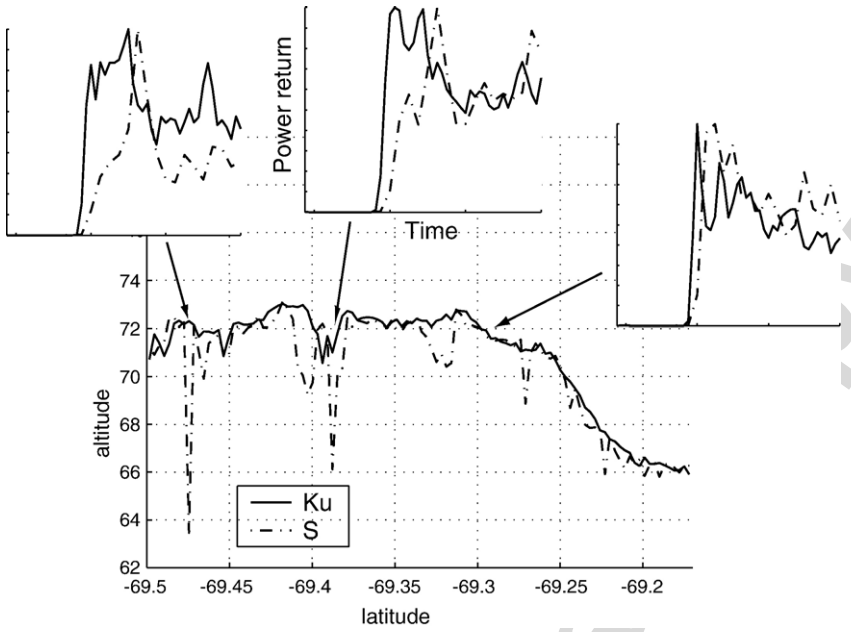

Fig. 2. Height measurement as measured by S (dashed line) and Ku (solid line). Radar altimeter waveforms are shown at three specific locations.

10–50 km. The altitude measurements show good agreement between S and Ku bands except at some specific points where the difference in altitude estimated between S and Ku bands is high. At these points, the measured altitude at S band is less than that at Ku band by between 3 and 9 m, while elsewhere this difference is within 0.8 m rms.

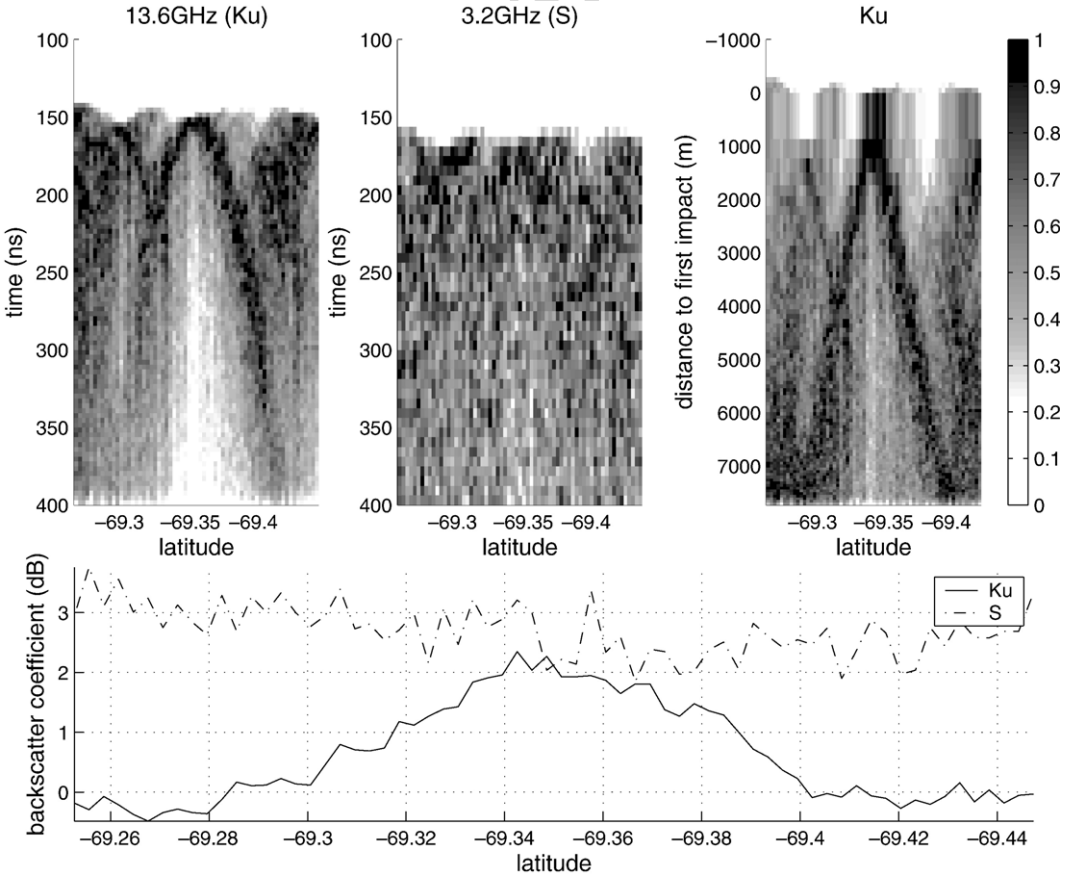

Fig. 3. Series of normalized waveforms above crevasses in time domain in Ku band (left), S band (middle) and series of Ku waveforms in distance to nadir domain (right). Bottom graph represents the backscatter coefficient evolution on the crevasse at Ku (solid line) and S band (dashed line). The waveforms are corrected for the antenna gain.

To investigate this phenomenon, the locations of points where the altitude difference ($h_{Ku} - h_S$) is greater than 3σ (the standard deviation of the altitude differences for each satellite track), are mapped on a MODIS image acquired at the same time as the altimetric data (January 2004, see Fig. 1). Looking at the MODIS image, it is clear that many of the points with large altitude difference are situated over crevasses. This is particularly obvious in the two parallel crevasse areas north of 70°15′S. In the southern part of the AIS, another area with a large spread of altitude anomalies is observed. This area displays many surface structures resembling melt streams and/or crevasses, even if crevasses are not clearly visible on the 250 m pixel resolution MODIS image. Altitude anomalies are also observed at the margins of the AIS, where topography is changing abruptly. Because of a larger beamwidth, S band is more sensitive to targets not directly situated at nadir, and therefore this band is more sensitive to ice-shelf margins where the profile moves from ice-shelf topography to steeper ice sheet slopes. However, over the whole MODIS image it is seen that most of altitude anomaly points are situated on crevasse features. The cause of this feature will be discussed in the Section 4.1.

2.3. Waveform series analysis

Over spatial scales of order 20 km, the series of Ku waveforms show several hyperbolas of high backscatter (Fig. 3, left) in the crevassed zone of the ice-shelf. These hyperbolic shapes are not seen in the S band records (Fig. 3, middle). The backscatter varies from 0 dB outside the hyperbola to 2 dB on the central part of the hyperbola in the Ku band, whereas the S band signal shows a constant backscatter of around 3 dB.

Hyperbolas are created by localised targets of high backscatter, or are due to a height difference between a target and its surrounding terrain (Nuth et al., 2002). The hyperbolic shape is thus created when the radar moves toward or away from the target. Firstly, we observe that the summit of the hyperbola is situated at or near the ice-shelf surface, implying that the position of the target is very close to the estimated surface obtained by the retracking algorithm. Moreover, it also indicates that the satellite is passing directly above the target. The analysis of the hyperbolic shapes from summer to summer shows that they are around the same position (see Section 3.1) and always situated within the crevassed areas. The ice-shelf at this location is moving at 950 m y^{-1} (Young & Hyland, 2002), but no account was taken of this movement over one season. Hyperbolas have often been observed in ground-penetrating radar data and attributed to sub-surface crevasses (e.g., Nath & Vaughan, 2003; Shabtaie & Bentley, 1987). In the following, we search for the origin of this signal in the altimetric data.

To retrieve the origin of this feature, the equation of the signal returned by an elongated target (modeling a linear crevasse) seen on a series of altimetric waveforms along the track is derived (Fig. 4). Let us consider the altimetric geometry

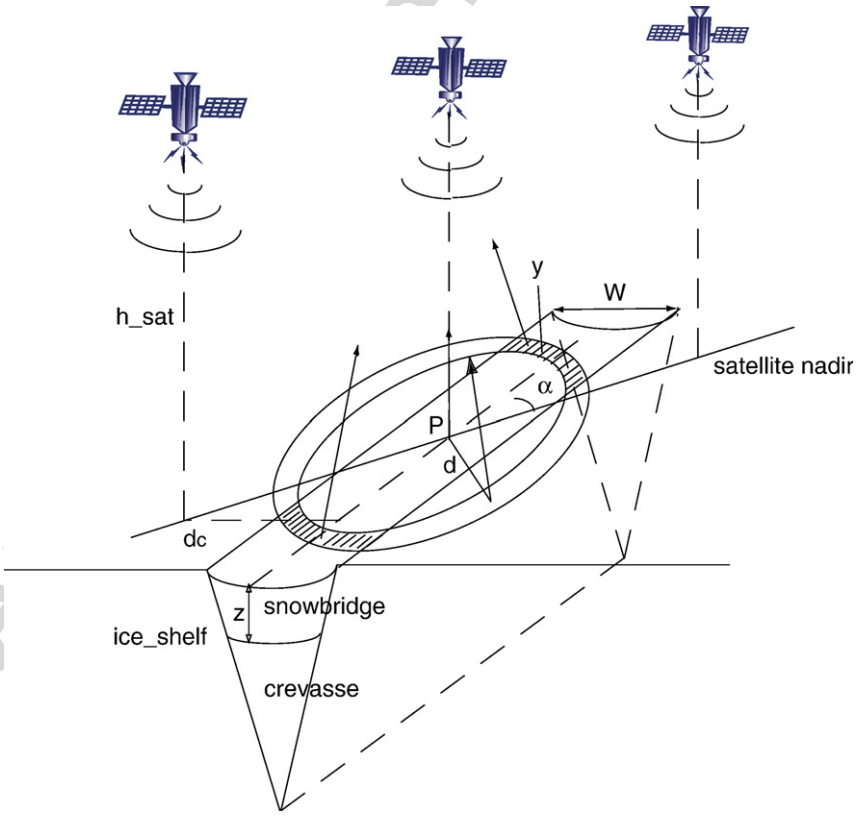

Fig. 4. Altimeter crossing a crevasse. The ring represent the surface illuminated by the radar at a time t_e, corresponding to a distance d from the nadir position. At that time the percentage of the ring surface on the crack is y. The crevasse is covered by a snowbridge of thickness z. The crack width is W. The satellite track cuts the crack with an angle α.

Table 2
Crevasse characteristics retrieved from the hyperbola method

Parameter	Left branch	Right branch
Angle α (°)	74	68
Target position (latitude, longitude)	(−69.346, 72.442)	(−69.337, 72.455)
Correlation coefficient	0.980	0.983

above crevasses: h_{sat} and v_{sat} are the satellite height and velocity, α the angle between the ENVISAT track and the target orientation. The distance d_c between target position and nadir at time T on the satellite track is given by:

$$d_c(T) = v_{sat}(T - T_0)\sin(\alpha) \quad (1)$$

with the origin of time T_0 taken when the target is situated at the nadir of the satellite.

At one specific location x, where x is the distance flown by the satellite ($x = v_{sat}.T$), the radar acquires a waveform. Because of coarse snow grains and relatively high temperatures in summer over the ice-shelf, penetration depth in Ku band is low (Matsuoka et al., 1996) and Ku echoes can be mostly considered as a single surface signal. This technique only works in summer (air temperature measured at the automatic weather station AM02 (69°42′48″S, 72°38′24″E) have been reaching up to 5 °C in December 2003, against below −30 °C in August). Moreover, Ku waveforms show values of trailing edge slope between $-1.0e^6$ s^{-1} and 0, which is in good agreement with a low signal coming from the sub-surface (see Section 3.1). Thus, the transformation between echo time t_e and distance to first impact d occurring at time t_s in the Ku waveforms can be derived as:

$$d(t_e) = \sqrt{\frac{2h_{sat}c(t_e - t_s)}{2} + \frac{(c(t_e - t_s))^2}{4}} \quad (2)$$

with c being the velocity of light in air.

In the new coordinate system (d, x), the elongated target is seen as a line of slope $v_{sat}\sin(\alpha)$. The cross-over between the line $d_c(x)$ and the point of the surface ($d=0$) corresponds to the position P of the target on the altimeter nadir.

The transformation is applied to the January 2004 ENVISAT waveform series and shown in Fig. 3 (right). Each branch of the hyperbola is processed separately by fitting a line on the transformed hyperbola to find both the angle α and the position of the target (Table 2). The cross-over between the two branches is situated at the position (lat, lon)=(−69.342°, 72.448°), and 30 cm below the surface altitude estimated by the Ku altimeter, which is consistent with a signal from the surface (30 cm is here less than one half of the leading edge width).

The two angles α are very similar, approximatively 70°, corresponding closely to the observed crevasses situated at this location (Fig. 1). Hence, we can conclude that the crevasse feature is the cause of this hyperbola signal.

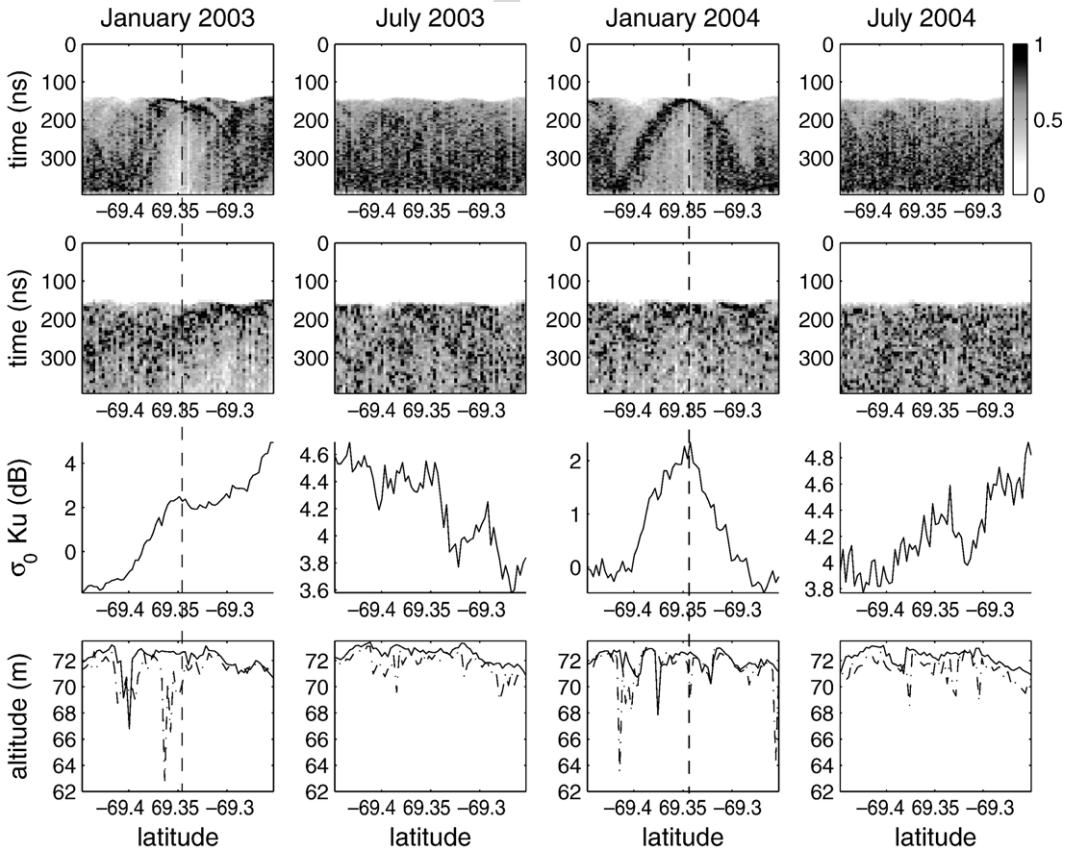

Fig. 5. Comparison of the waveform signal between summer and winter. From left to right: January 2003, July 2003, January 2004, July 2004. From top to bottom: series of normalized waveforms above crevasse at Ku band, at S band, backscatter evolution at Ku band, height measurement as measured by S (dashed line) and Ku (solid line).

3. Hyperbola analysis

3.1. Seasonal analysis of the altimetric signal and properties of the surrounding shelf

The altitude record in winter (Fig. 5) shows that the previous characteristics of the signal are only visible in summer. Indeed, discrepancies of ($h_{Ku}-h_S$) in winter still exist but the amplitude is much lower (less than 2 m in winter compared to 3 to 9 m in summer). This means that crevasses have a much lower impact on the altimetric signal compared to the background signal in winter than in summer. This is also strengthen by looking at the seasonal variability of the backscatter signal (Fig. 5). Indeed, at Ku band, the backscatter varies between around 4 dB in winter and 0 dB in summer, due to melt events (Fricker et al., 2005). We notice that the hyperbola is seen only when the mean backscatter at Ku band is low. Certainly, during wintertime, the hyperbola signal does not disappear but is drowned in the higher background backscatter.

The trailing edge slope at Ku band is low in summer ($-1e^6$ s^{-1}) but rises up to $1.0e^6$ s^{-1} in winter. The backscatter at S band does not follow clear seasonal variations. In summer, the S band trailing edge slope is very low ($-2.5e^6$ s^{-1}), increasing to $-1e^6$ s^{-1} during the rest of the year, which is still low. These observations are consistent with the fact that the S band signal on the ice-shelf is minimally influenced by the scattering snow medium, and is mostly a signal from the surface. The low trailing edge slope is related to the fact that the snow surfaces reflect more energy at nadir than off-nadir.

The increase of snow temperature decreases the radar wave penetration and consequently the backscatter from the snow-pack. As a result, the trailing edge slope on the Ku and S waveforms is lower. At the same time, melting smooths the snow surface, which impacts the trailing edge slope in the same manner, but contributes to more backscatter energy at nadir. This effect is more important at lower frequencies. Thus the drop of backscatter from the lower penetration in summer at S band is balanced by the increase of surface backscatter, which can explain the seasonal evolution of the S band signal.

The positive values of trailing edge slope observed at Ku band in winter on the noncrevasse-perturbated part of the shelf indicate that there is a small but significant volume contribution to the radar waveforms. Because of specular waveforms at S band, the volume contribution cannot come from layering or ice-lens signals. Indeed, due to its higher penetration depth, S band waves would be even more sensitive to the layering by ice-lenses than Ku waves, and we would also expect to see a high trailing edge (which is not the case). We therefore conclude that the scattering by snow grains is at the origin of this observed volume signal.

3.2. Separation between crevasse and background signal

To understand why the Ku radar is sensitive to the crevasse, we try to separate the effect of the crevasse from its surrounding properties, based on the hyperbola signal. The surface area of the radar ring is constant (Fig. 4), but its width decreases the further we are from the nadir. Thus the crevasse surface covers more radar bins if located far from the nadir than just below the satellite. The crevasse is modelled by an elongated target of width W, as shown in Fig. 4. The ratio y between the crevasse surface and the radar ring surface S when the echo is situated at distance d from the nadir (corresponding to time t_e in the waveform) is calculated based on the surface area of a circle intersected by an infinitely long rectangle:

$$y(t_e)=\frac{d(t_e)^2*\left[\left(a\cos\left(\frac{d_c-W/2}{d(t_e)}\right)-\sin\left(a\cos\left(\frac{d_c-W/2}{d(t_e)}\right)\right)\right)-\left(\left(a\cos\left(\frac{d_c+W/2}{d(t_e)}\right)-\sin\left(a\cos\left(\frac{d_c+W/2}{d(t_e)}\right)\right)\right)\right]}{S} \quad (3)$$

where, d_c is the distance between the crevasse and the nadir point.

At each time t_e in the waveform, the backscatter is an average of crevasse backscatter σ_0^c and its surrounding σ_0^s weighted by y, as follows:

$$\sigma_0(t_e)=\sigma_0^c y(t_e)+\sigma_0^s[1-y(t_e)]. \quad (4)$$

For each waveform, d_c is known from previous processing (Section 2.3 and Eq. (1)), and d is calculated using Eq. (2). The difference between observed and modelled σ_0 is minimized for each radar bin in the waveform using a least squares solution to find W, σ_0^c and σ_0^s. With this processing, we separate the crevasse effect from the background ice-shelf signal.

The mean σ_0^s is found to be 1.2 dB±15%. The crevasse width is estimated to be W=281 m±91 m. This value is consistent with the width measured on a Radarsat image with a 30 m resolution (the image shows a 300 m crevasse). The crevasse backscatter σ_0^c is not constant for varying waveforms, and decreases from 12 dB to less than 9 dB. Because of the small size of the crevasse compared to the radar footprint, the crevasse is seen with varying incidence angles as the satellite approaches or retreats the crevasse. Thus, retrieving σ_0^c for different waveforms provides the radiation pattern $\sigma_0^c(\theta)$ of the crevasse surface, when the incidence angle θ varies around 0° incidence (Fig. 6).

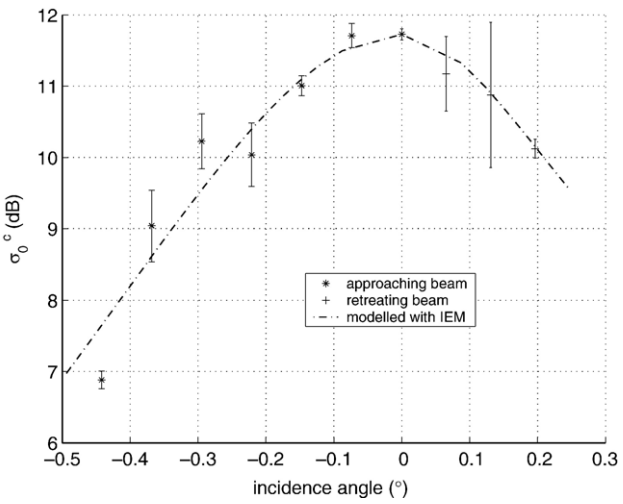

Fig. 6. Radiation pattern of the crevasse around 0° incidence, measured with the approaching (star) and retreating beams (cross).

3.3. Physical interpretation

The large crevasses responsible for the observed hyperbola shape have been flown over with helicopter surveys during several AIS summer field seasons between 2002 and 2006. They have always been observed to be filled with snow at the start of the austral summer season — September to December. Thus, in the following discussion we investigate different scenarios to explain these differences of backscatter behaviour between the two bands: a/ effect of snow grain scattering or coarse hoar crystals in the snowbridge; b/ sensitivity to snow roughness at the snowbridge surface; c/ effect of the crevasse geometry.

3.3.1. Snow grain scattering effects

Fig. 6 shows a rapid decrease of backscatter with incidence angle, and a very high backscatter at 0° incidence of almost 12 dB. These two observations exclude the hypothesis of scattering by snow grains for two reasons. Firstly, the volume scattering of snow is independent of the look angle over the range considered. Secondly, the snow grain scattering does not produce such high backscatter coefficients. We follow Matzler (1987) to express the backscatter coefficient σ_0^v of a volume V of freely arranged spheres of ice embedded in an air medium:

$$\sigma_0^v = k_s \int_0^{\delta} \exp^{(-(k_a+k_s)dz)} dz \tag{5}$$

$$k_a = v k_0 \epsilon'' \left| \frac{2\epsilon_{eff}+1}{2\epsilon_{eff}+\epsilon'} \right|^2 \tag{6}$$

$$k_s = 3 p_c^3 \frac{k_0^4}{32} v(1-v) \left[(\epsilon'-1) \frac{(2\epsilon_{eff}+1)}{(2\epsilon_{eff}+\epsilon')} \right]^2 \tag{7}$$

where δ is the penetration depth, related to the attenuation (k_a) and scattering (k_s) coefficients. The effective permittivity of snow ϵ_{eff} is provided by the Polder and van Santen formula (1946), p_c the volume correlation length in the media, ϵ' and ϵ'' the real and imaginary parts of the dielectric permittivity of ice, v the volume fraction of ice with in the media, k_0 the wavenumber in the air. v and p_c are related to an effective grain radius r. This equation is equivalent to a Rayleigh diffusion law with a corrective factor related to p_c. Using Eq. (5), σ_0^v is computed for different grain sizes. A series of such estimates shows σ_0^v is limited to maximum values around 5 dB in Ku band. Thus, the scattering by snow grains cannot explain a 12 dB backscatter at nadir.

3.3.2. Surface roughness effects

The hypothesis of surface scattering is strengthened by the radiation pattern aspect. Indeed, rapid decrease of σ_0^c away from the vertical, and strong backscatter coefficients are in agreement with specular surface radiation pattern, with an important coherent component visible at nadir.

Using the integral equation method (Fung, 1994), we compute the backscatter for different incidence angles around the vertical for surfaces with varying roughness parameters (σ_h, l). The σ_h is the rms of the surface height distribution, usually assumed to be Gaussian and l is the surface correlation length. The auto-correlation function of the snow surface is here assumed to be an exponential. The residuals between measured and modelled backscatter for different incidences is minimized (Fig. 6). The least squares solution provides a surface of roughness characteristics: (σ_h, l)=(4 mm, 28 cm), which are the characteristics of a smooth surface, with a strong specular component at Ku band. The backscatter that this surface would return at S band is then computed. A 3.2 dB value at 0° incidence is found, which is close to the averaged backscatter found in this area (3 dB). Thus, the crevasse is not sufficiently contrasted with its surroundings to be distinguished by the S band radar. This could explain why no hyperbolic shape is visible on the S band waveform series. However, this hypothesis imposes that a natural process creates a different roughness at the snowbridge surface than outside the crevasse.

3.3.3. Geometric effects

Because the hyperbola is seen from summer to summer, it is also thought that the specific scattering of the crevasses can be created by a particular geometry. 1/the parabolic-shaped trough induced by the snowbridge weight on the crevasse (that allows the snowfilled crevasse to be detected by optical sensors), can concentrate the energy and create preferential scattering directions. This trough can also play the role of a corner reflector at the borders of the crevasse and then increase the backscattered signal. 2/the relatively sharp edge of the crevasse, can also create preferential scattering directions (e.g. Dano, 2001). Nevertheless, the case is not well documented for vertical incidences, and the hypothesis must be investigated in more detail.

As seen on the seasonal analysis (Section 3.1), the background backscatter at Ku band masks the crevasse signal in winter. In the same manner, the natural high background backscatter at S band can mask the existing crevasse signal throughout the year. This is the reason why we cannot make definitive statements about the origin of this hyperbola signal. However, we can relate it to a crevasse feature and characterize its effect on the Ku signal such that it allows us to describe the scattering properties of the crevasses.

4. S band echo analysis

4.1. Evidence of sub-surface echo and physical interpretation

As seen in Fig. 5, we notice that the two signals used to detect the crevasses (hyperbola at Ku band and anomalies in the altitude estimated by the S band) match quite well in summer. Indeed, the crevasse detected with the hyperbola corresponds to a difference $h_{Ku} - h_S$ of more than 3 m. The hyperbola was originated by a process situated on the surface. We consider if the source of the second signal is also coming from the same physical processes. To achieve our goal, we look at the waveforms showing discrepancies in altitude between the S and Ku bands.

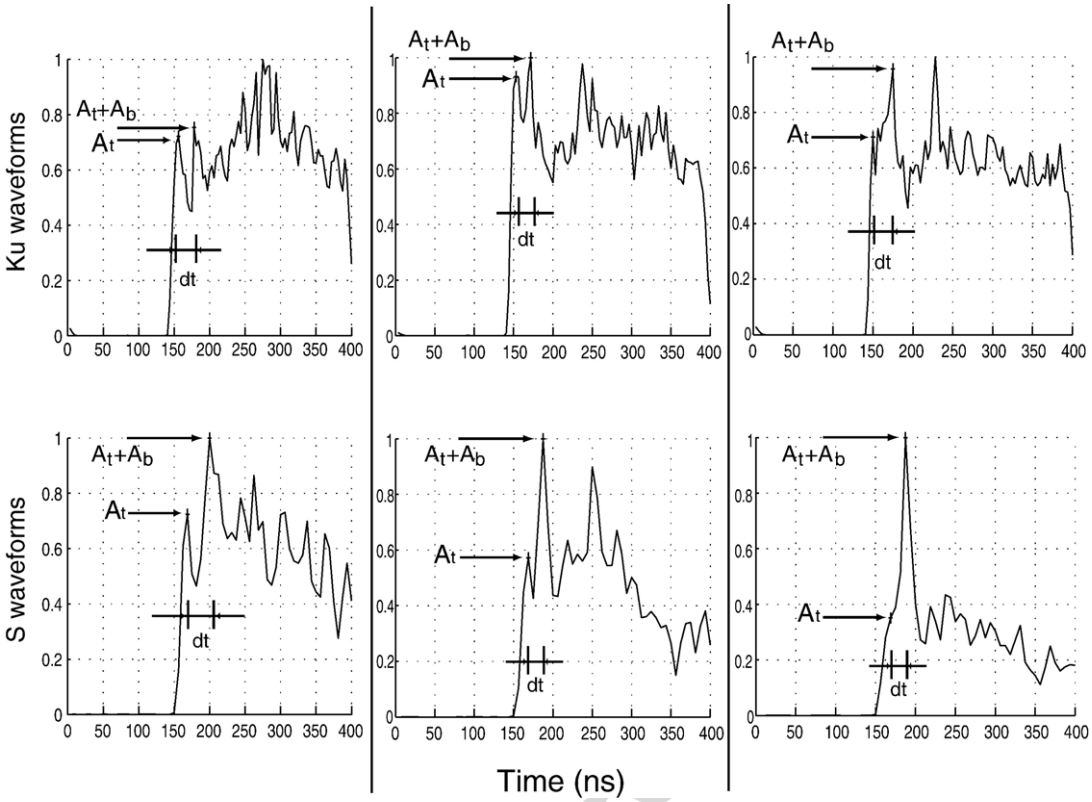

Fig. 7. Ku (top) and S (bottom) waveforms above crevasses. The two echoes are depicted in each waveform. The time interval d*t* between the two echoes provides the snowbridge thickness. Then, the amplitudes A_t and A_b provide the extinction coefficient.

These differences are caused by a longer leading edge in the S waveforms than in the Ku ones above crevasses (Fig. 7). The leading edge above crevasses in S band often shows a double edge, a feature that can also be seen in some Ku waveforms, but with a lower amplitude. We interpret this double edge as a signal coming from the sub-surface. Indeed, above crevasses, where the Ku band remains mostly sensitive to the surface due to the low penetration in summer, the Envisat S band altimeter acts differently. S band waves are much less attenuated by the snow and penetrate deeper into the firn. The presence of a snowbridge above the crevasse adds volume signal. The snowbridge bottom delimits a second interface between snow and air. This interface creates a second echo in the S band waveform at the origin of this double edge. This effect causes a longer leading edge when the waveforms are retracked. Thus the altitude estimated with the S band altimeter is lowered.

Moreover, this effect is only visible in summer because of the specularity of the summer surfaces, that makes the altimetric signal mostly sensitive to the snow situated at nadir (see Section 3.1). The relative importance of the reflections at nadir is higher in summer than in winter. The amplitude of the second echo is often much higher than the mean background echo level. Further, the bottom interface area S_b is smaller than the top surface area S_t (the ratio defined by Eq. (3) is always smaller than 1. This is of course not true anymore for very large rift zones, where their widths can exceed 2000 m). This leads us to conclude that the backscatter coefficient of the snowbridge bottom σ_{0b} is much higher than the backscatter coefficient of the surface σ_{0t}. This high backscatter is caused either by a high density contrast at the interface between the snowbridge bottom and air below or by a specular interface, or maybe both. The surface is certainly specular because the echo is not seen in the waveforms outside crevasses. An explanation can be that the interface between the snowbridge bottom/air is composed of a layer of ice caused by the refreezing of melted snow at the contact of cold air under the snowbridge.

4.2. Extinction coefficient

The waveform analysis above crevasses showed for the first time that we can retrieve sub-surface echoes in the individual waveforms. This sub-surface echo is high at S band due to its higher penetration depth, but can also be detected on the Ku waveforms, though it is attenuated by the snow (Fig. 7). Hence, by looking at the amplitude difference between the two echoes for each radar band, the snow extinction on the ice-shelf can be assessed.

The amplitude ratios between echoes from the top (A_t) and bottom (A_b) of the snowbridge are assumed to be the same in S and Ku band once corrected for their respective extinction coefficients k_{eS} and k_{eKu}:

$$\left.\frac{A_b}{A_t}\right|_{Ku} \exp^{2k_{eku}z} = \left.\frac{A_b}{A_t}\right|_{S} \exp^{2k_{eS}z} \tag{8}$$

where A_t and A_b are the reflection amplitudes at the surface and the bottom of the snowbridge, and z the snowbridge thickness.

The extinction coefficient in S band is much smaller than in Ku, and can, to first order, be neglected. Depicting the two echoes in each waveform provides A_t, A_b and dt, the time interval between the two echoes (Fig. 7), where dt is related to z by assuming a constant electromagnetic speed in the snow of $\frac{c}{1.3}$, corresponding to a mean snow density of 0.35 g cm^{-3}.

Then k_{eKu} is found through the equation:

$$k_{eKu} = -\frac{1}{2z} * \log\left[\frac{A_b}{A_t}\bigg|_{Ku} \frac{A_t}{A_b}\bigg|_{S}\right]. \quad (9)$$

The method is applied to a number of waveforms clearly showing a double edge, including the waveforms from the hyperbola. For the series of waveforms from the hyperbola area, because the echo A_t at Ku band is not related to the mean surface echo (Section 3.3 and Eq. (4)), the amplitude A_t is not the first echo but the mean of the waveform amplitude in the trailing edge slope. The snowbridge thicknesses are found to be in the range between 1.8 m and 7.2 m with the Ku signal and between 2.1 m and 7.2 m with the S band. The thicknesses are similar for the two bands, meaning that the two echoes retrieved by the method at Ku band are well correlated with the two echoes retrieved in S band. These values are in general agreement with field observations near the front of the ice-shelf, where probes made with a crevasse pole show values of snowbridge thickness around 3–4 m.

The extinction coefficient found with this method applied to the waveforms on crevasses exhibiting or not an hyperbola compared very well together. The extinction coefficient is found to be k_{eKu}=0.18±0.04 Np m^{-1} leading to a 5.7 m±1.2 m penetration depth. However k_{eKu} is underestimated due to the assumption of no extinction in the S band. Other studies (Arthern et al., 2001; Legrésy & Rémy, 1998) on Antarctic snow showed penetration depths at Ku band of between 5 and 12 m. The 5.7 m value found here is thus in good agreement with the lower limit of this range. This low value is due to the high summer temperatures (up to 5 °C measured at AM02 weather station at the end of December 2003), and the coarse grains induced by a strong temperature gradient in the snowbridge.

5. Conclusion

The presence of snowfilled crevasses within ice-shelves modifies the signal homogeneity in these flat areas. Indeed, differences of snow characteristics and geometric properties of crevasses compared to the firn outside crevasses make crevasses a completely distinguishable target for radar waves influenced by both backscatter coefficient contrast and differences of penetration properties. The snowfilled crevasses are detected by hyperbolas of high backscatter in the series of Ku waveforms along the track, and altitude bias at S band.

The seasonal analysis of these signals shows that crevasses are detected by the radar only in summer for two main reasons: 1/ the backscatter of the surrounding ice-shelf is lower in summer, making the crevasse signal relatively more important. The lower backscatter in summer is caused by a lower radar penetration into the snow medium. 2/ the smooth surfaces caused by the summer melting make the radar signal mostly sensitive to the nadir echoes.

The Ku radar detects the crevasses largely due to their surface scattering characteristics being different from the surrounding ice-shelf. The crevasse reflects more energy, possibly due to wedge scattering at the crevasse corners or the snowbridge-induced trough or due to a particular snow surface roughness on the snowbridge. We used these features to assess the geometric properties of the snowfilled crevasse (width and orientation). The detection is limited by the low spatial resolution of the altimeter. However, we used the signal at Ku band to characterize the scattering properties of the crevasse, using a method that can be applied to any small size targets compared to the altimeter footprint.

The comparison of the altitude series between Ku and S bands, brings for the first time the proof of sub-surface echoes in the individual altimetric waveforms in Antarctica. The observed echoes are shown to be a reflection from the snowbridge bottom, that allow us to calculate snowbridge thicknesses. We also used this waveform characteristic to assess a penetration depth at Ku band in the snowbridge during summer months, which is found to be 5.7 m. This is in agreement with the penetration depth previously estimated at Ku band on the Antarctica plateau. The summer snow conditions described here, correspond well with regions where melting occurs (either Antarctic borders or most of the Greenland ice-cap). We can therefore hope to find and follow sub-surface echoes everywhere in these regions using the dual-frequency altimeter of Envisat.

Finally, we showed that, even with a low resolution dual-frequency altimeter, we cannot only detect crevasses (which are easily identified with optical images in summer, or with SAR images) but also retrieve their geometric and scattering properties.

In the future, better resolution radar systems, such as Cryosat (250 m wide along track resolution in SAR mode) or dedicated multiple frequency radars onboard aircraft, would make possible seasonal studies of the crevasse characteristics, leading to new understanding of the dynamics of ice shelves.

Acknowledgements

This work is a contribution to the RAIES ENVISAT RA-2 project, and to the OSCAR project. The authors would like to thank Ted Scambos for his very constructive comments on this study. This work also benefited from the useful remarks of Bernard Pirletta.

References

Arthern, R. J., Wingham, D. J., & Ridout, A. L. (2001). Controls on ERS altimeter measurements over ice sheets : Footprint-scale topography, backscatter fluctuations, and the dependence of microwave penetration depth on satellite orientation. *Journal of Geophysical Research*, *106*(D24), 33.471–33.484.

Dano, E. B. (2001). Radar backscatter from mechanically generated transient breaking waves. *IEEE Journal of Oceanic Engineering*, *26*(2), 181–200.

Fahnestock, M. A., Abdalati, W., & Shuman, C. (2002). Long melt seasons on ice shelves of the Antarctic Peninsula: An analysis using satellite based microwave emission measurements. *Annals of Glaciology*, *34*, 127−133.

Fricker, H. A., Young, N. W., Coleman, R., Bassis, J. N., & Minster, J. B. (2005). Multi-year monitoring of rift propagation on the Amery Ice Shelf, East Antarctica. *Geophysical Research Letters*, *32*(2), L02502. doi:10.1029/J2004GL021036

Fung, A. K. (1994). *Microwave Scattering and Emission Models and Their Applications.* Boston, MA: Artech House.

Hawley, R. L., Morris, E. M., Cullen, R., Nixdorf, U., Shepherd, A. P., & Wingham, D. J. (2006). ASIRAS airborne radar resolves internal annual layers in the dry-snow zone of Greenland. *Geophysical Reseach Letters*, *33*, LO4502. doi:10.1029/J2005GL025147

Jun, L., & Zwally, H. J. (2002). Modeled seasonal variations of firn density induced by steady-state surface air-temperature cycle. *Annals of Glaciology*, *34*, 299−302.

Legrésy, B., & Rémy, F. (1997). Surface characteristics of the Antarctic ice sheet and altimetric observations. *Journal of Glaciology*, *43*(14), 265−275.

Legrésy, B., & Rémy, F. (1998). Using the temporal variability of the radar altimetric signal to map surface characteristics of the Antarctic ice sheet. *Journal of Glaciology*, *44*(147), 197−206.

Legrésy, B., Papa, F., Rémy, F., Vinay, G., Van den Bosh, M., & Zanife, O. Z. (2005). ENVISAT radar altimeter measurements over continental surfaces and ice caps using the ICE-2 retracking algorithm. *Remote Sensing of Environment*, *95*, 150−163.

Legrésy, B., Rémy, F., & Schaeffer, P. (1999). Different ERS altimeter measurements between ascending and descending tracks caused by wind induced features over ice sheets. *Geophysical Research Letters*, *26*(15), 2231−2234.

Matsuoka, T., Fujita, S., & Mae, S. (1996). Effect of temperature on dielectric properties of ice in the range 5–39 GHz. *Journal of Applied Physics*, *80* (10), 5884−5890.

Matzler, C. (1987). Applications of the interaction of microwaves with the natural snow cover. *Remote Sensing Reviews*, *2*, 259−387.

Nath, P. C., & Vaughan, D. G. (2003). Subsurface crevasse formation in glaciers and ice sheets. *Journal of Geophysical Research*, *108*, 10.1029−10.1041.

Nuth, V., Pulliam, J., & Wilson, C. (2002). Migration of radar altimeter waveform data. *Geophysical Research Letters*, *29*(10), 131.1−131.4.

Phillips, H. A. (1998). Surface meltstreams on the Amery Ice Shelf, East Antarctica. *Annals of Glaciology*, *27*, 177−181.

Polder, D., & van Santen, J. H. (1946). The effective permeability of mixtures of solids. *Physica*, *12*(5), 257−271.

Rémy, F., Mazzega, P., Houry, S., Brossier, C., & Minster, J. F. (1989). Mapping of the topography of continental ice by inversion of satellite-altimeter data. *Journal of Glaciology*, *35*(119), 98−107.

Ridley, J. K., & Partington (1988). A model of satellite radar altimeter return from ice-sheets. *International Journal of Remote Sensing*, *9*(4), 601−624.

Scambos, T., Hulbe, C., Fahnestock, M., & Bohlander, J. (2000). The link between climate warming and break-up of ice shelves in the Antarctic Peninsula. *Journal of Glaciology*, *46*, 510−530.

Shabtaie, S., & Bentley, C. R. (1987). West Antarctic ice streams draining into the Ross Ice Shelf configuration and mass balance. *Journal of Geophysical Research*, *92*, 1311−1336.

Shepherd, A., Wingham, D., Payne, T., & Skarva, P. (2003). Larsen ice shelf has progressively thinned. *Science*, *302*, 856−859.

Young, N. W., & Hyland, G. (2002). Velocity and strain rates derived from InSAR analysis over the Amery Ice Shelf, East Antarctica. *Annals of Glaciology*, *34*, 228−234.